	Form Approved OMB NO. 0704-0188

1. AGENCY USE ONLY (Leave Blank)	2. REPORT DATE	3. REPORT TYPE AND DATES COVERED
	April 17, 2007	Final Progress Report 15 Feb 06 - 31 Dec 06

4. TITLE AND SUBTITLE	5. FUNDING NUMBERS
Reversible Control of Anisotropic Electrical Conductivity Using Colloidal Microfluidic Networks	Agreement # W911NF-06-1-0050
6. AUTHOR(S) Ali Beskok, Michael Bevan, Dimitris Lagoudas, Zoubeida Ounaies	
7. PERFORMING ORGANIZATION NAME(S) AND ADDRESS(ES) Texas Engineering Experiment Station	8. PERFORMING ORGANIZATION REPORT NUMBER
9. SPONSORING / MONITORING AGENCY NAME(S) AND ADDRESS(ES) U. S. Army Research Office P.O. Box 12211 Research Triangle Park, NC 27709-2211	10. SPONSORING / MONITORING AGENCY REPORT NUMBER 50508.1-MS-DRP

11. SUPPLEMENTARY NOTES

The views, opinions and/or findings contained in this report are those of the author(s) and should not be construed as an official Department of the Army position, policy or decision, unless so designated by other documentation.

12 a. DISTRIBUTION / AVAILABILITY STATEMENT	12 b. DISTRIBUTION CODE
Approved for public release; distribution unlimited.	

13. ABSTRACT (Maximum 200 words)

This research addresses the tunable assembly of reversible colloidal structures within microfluidic networks to engineer multifunctional materials that exhibit a wide range of electrical properties. Our work has focused on studying electric field-directed assembly of gold colloids and understanding how tuning colloidal configurations can be utilized to modulate electrical properties within a microfluidic electric circuit. More specifically, we have found that a single circuit element can act as a variable resistor, capacitor, and inductor by regulating the colloidal structures within the gap between electrodes. Navigating the applied AC voltage-frequency phase space allows us to probe a wide range of colloidal configurations that resemble "capacitive" and "resistive" networks in their limiting cases. All colloidal configurations formed were reversible and repeatable, and it was possible to switch from one configuration to other interchangeably. Based on a scaling analysis, different electrokinetic forces that drive assembly have been identified. The scaling analysis was able to consistently interpret experimental observations of particle dynamics over the planar electrode system, and can be extended, within limits, to more complex electrode geometries for future studies.

14. SUBJECT TERMS	15. NUMBER OF PAGES
Microfluidics, Colloidal Systems, Electrical Properties	13
	16. PRICE CODE

17. SECURITY CLASSIFICATION OR REPORT	18. SECURITY CLASSIFICATION ON THIS PAGE	19. SECURITY CLASSIFICATION OF ABSTRACT	20. LIMITATION OF ABSTRACT
UNCLASSIFIED	**UNCLASSIFIED**	**UNCLASSIFIED**	**UL**

NSN 7540-01-280-5500

Standard Form 298 (Rev.2-89)
Prescribed by ANSI Std. 239-18
298-102

TABLE OF CONTENTS

Statement of the Problem Studied **2**

I. Experimental 3

Ia. Materials and Methods 3

Ib. Fabrication of planar gold electrodes 3

Summary of the Most Important Results **4**

II. Exploring colloidal configurations in the voltage-frequency phase space – transition from capacitive to resistive behavior 4

III. Scaling analysis. 6

IV. Electrical property measurements 9

Listing of all Publications **13**

List of all participating scientific personnel **13**

Reversible Control of Anisotropic Electrical Conductivity using Colloidal Microfluidic Networks

Statement of the Problem Studied

This research addresses the tunable assembly of reversible colloidal structures within microfluidic networks to engineer multifunctional materials that exhibit a wide range of electrical properties. Future integration of these devices into proven technology, such as electronically reconfigurable surfaces, will provide a significant enhancement in overall performance, and extend current technological capabilities. However, prior to applying this work to directly impact existing technology, we seek to gain a fundamental understanding of the phenomenological aspects of how electrical property changes are related to colloidal configurations. Furthermore, we also envision that findings from this research will have a broad significance to technologies seeking to actively assemble active nano- and micro- structured materials on macroscopic substrates to control electrical, thermal, mechanical and magnetic properties.

Our work has focused on studying electric field-directed assembly of gold colloids and understanding how tuning colloidal configurations can be utilized to modulate electrical properties within a microfluidic electric circuit. More specifically, we have found that a single circuit element can act as a variable resistor, capacitor, and inductor by regulating the colloidal structures within the gap between electrodes. Navigating the applied AC voltage-frequency phase space allows us to probe a wide range of colloidal configurations that resemble “capacitive” and “resistive” networks in their limiting cases (low frequency & high voltage, and high frequency & high voltage, respectively). All colloidal configurations formed were reversible and repeatable, and it was possible to switch from one configuration to other interchangeably. Based on a scaling analysis, the different electrokinetic forces that drive assembly (electrophoresis, AC electroosmosis, and dielectrophoresis) have been assigned to frequency and voltage domains that dictate (i) the types of colloidal structures assembled, (ii) whether they form or break apart, and (iii) the rates at which forward and reversible assembly occur. In addition, the scaling analysis was able to consistently interpret experimental observations of particle dynamics over the planar electrode system, and can be extended, within limits, to more complex electrode geometries in the future.

Thus far, colloidal structures within the electrode gaps have taken on the form of 1) spanning nanowires that bridge the gap between the electrodes (variable resistor/switch mode), 2) non-spanning assemblies that vary the dielectric properties of the gap (variable capacitor mode), and 3) spanning wires with induced current from superimposed AC electroosmosic flow of ions (variable inductor mode). The resistance of the circuit dropped to a low value of about 300 Ohms when configuration 1 evolved from a random configuration of Brownian colloids. The results for configuration 2 showed a four fold increase in capacitance from its base-line value obtained under zero external forcing. Extensive measurements of the circuit inductance associated with configuration 3 were not made in this study and is planned for future work. A greater theoretical understanding that allows predictive capability of how electrical properties change with colloidal configurations, is essential for the design of robust multifunctional materials in the future. Nevertheless, this work conclusively demonstrates our ability to change the impedance characteristics of the system by facilitating a change in the colloidal configuration.

Current work is centered on devising new electrode geometries to enhance performance by assembling and reversing structures faster and through the creation of more varied colloidal structures. Furthermore, other microfluidic circuit elements that utilize colloidal property changes are being pursued to create more powerful variable inductors that complement our existing devices. Integrating microfluidic systems with structural composites will enable a new class of multifunctional hybrid materials, in which new capabilities (optical, magnetic, electrical, self-healing, etc.) will offer superior applications to DoD’s needs in the areas of optics, smart materials, electronics, and sensors.

I. Experimental

Ia. Materials and Methods

Nominal 800 nm gold colloids (Alfa Aesar., Ward Hills, MA) with a reported density of ρ_{Au}=19,000 g/ml were diluted in a 0.1 mM sodium bicarbonate ($NaHCO_3$) ionic solution to obtain bulk particle concentrations that produced desired interfacial concentrations after sedimentation equilibrium was attained. The ionic solutions were prepared with ~ 15 MΩ de-ionized (DI) water. An Agilent 33120A function generator was used to apply an alternating potential (ω=10 Hz – 1 MHz, voltage=0.5 V – 2.5 V peak to peak) to the microfluidic cell. Silver filled epoxy dots were used to provide the electrical connections to the electrodes. Reversing the electrical connections to the electrodes produced no change in the measured behavior, which means there was zero DC bias in the electronics. A Tektronix TDS210 two channel oscilloscope monitored the applied AC signal. An Agilent 4194A impedance analyzer was used to record the electrical properties (impedance, phase-angle, capacitance and resistance) of the different colloidal configurations formed in the microfluidic cell as a function of frequency.

The two-dimensional Brownian excursions of the colloidal particles were monitored using standard Video Microscopy (VM) techniques. Video Images were obtained using a 40X (NA=0.75) objectives (Zeiss, Germany), in conjunction with a 12 bit CCD camera (ORCA-ER, Hamamatsu, Japan) operated with 2X binning. A sequence file of equilibrium particle configurations was generated at 18 frames/s with 672 x 512 resolution to produce 303 nm pixels.

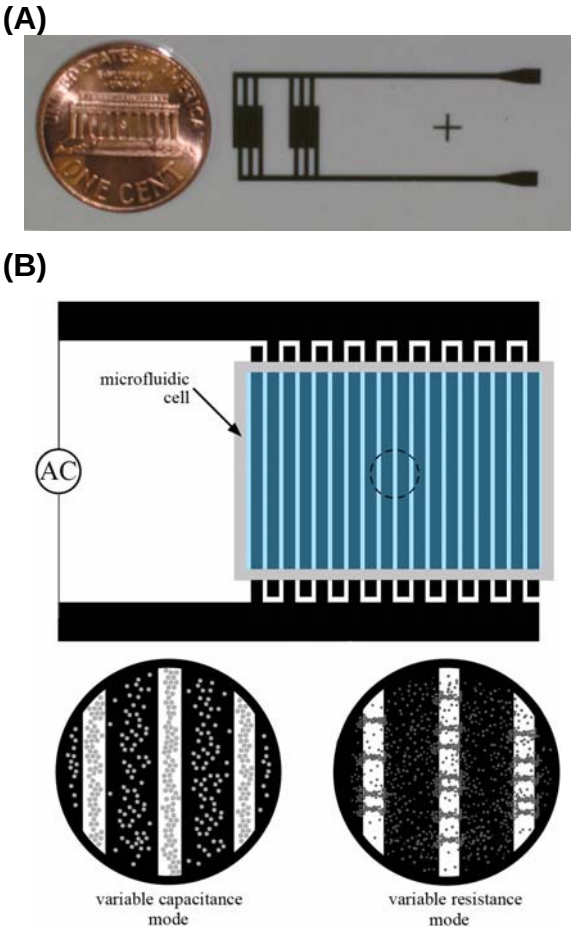

Figure 1. (A) Photograph of the interdigitating gold electrode patterned on a glass substrate using standard photolithography, (B) Schematic representation of the microfluidic cell used in experiments. The two "zoomed" views represent the phenomena of capacitive changes brought about by assembly within the center of the gap that varies the dielectric permittivity of the spanning fluid (left) and the variable resistance and switch behavior of metal particles assembling into wires that span the electrode gap in the presence of a AC field (right)

Ib. Fabrication of planar gold electrodes

Conventional photolithographic techniques were used to create the patterned electrodes generating colloidal configurations with variable and reversible electrical properties (Fig. 1A). To begin, microscope glass slides were immersed in a 3:1 mixture of H_2SO_4 to 35% H_2O_2 for 1 hour to remove organic contaminants. Slides were then rinsed thoroughly with DI water and blown dry with air. An S1813 photoresist layer (~1.5 μm thick) was applied to the slides by dispensing 1 ml of photoresist onto the preheated (115 ºC) glass substrates and spinning at 3000 rpm for 30 seconds. The photoresist was soft baked on a hotplate for 60 seconds at 90 ºC and then exposed to ultraviolet (UV) light through a patterned chrome mask for 4 seconds. Before being immersed in MF 319 developer for 60 seconds, the UV-exposed photoresist film was post baked for 120 seconds at 115 ºC. Following development, the photoresist pattern was placed in a reactive ion etcher (CS-1701, March

Plasma Systems, CA) and exposed to oxygen plasma for 30 seconds at 200 W with an O_2 flow rate of 0.3 cm^3/s to remove any photoresist and developer residue on the glass regions. Patterned slides were placed in a metal evaporator chamber (BOC Edwards, Auto306) and 5nm of Chrome (Cr) then 50nm of gold (Au) were deposited onto the slides at a rate of 1.0 Å/s. Lift off of the patterned Au electrodes was achieved by ultrasonicating the Au-coated photoresist pattern in acetone for 10 minutes to remove the underlying photoresist.

The same electrode design was utilized to engineer the colloidal RF switch and variable capacitor devices. Figure 1B shows a schematic view of the interdigitating gold electrodes (average spacing between electrodes ~ 30 μm) used in all experiments reported here. A microfluidic cell containing a dispersion of gold nanoparticles in an ionic solution is sandwiched between the interdigitating electrodes at the bottom and a glass cover slide on top. The microfluidic device has two operation modes depending on the colloidal configuration assumed by the metallic nanoparticles: 1) variable capacitor, and 2) variable resistor, and it can reversibly and rapidly switch between the two modes (Fig. 1B). Growth of colloidal wires spanning the gap between the two electrodes, establishes a conductive network circuit, and variable resistance can be realized by controlling the growth and the number of colloidal wire interconnects. A variable capacitive circuit can be realized by concentrating colloidal particles in between the electrodes that change the effective spacing between the electrodes, and thereby the capacitance. For a given concentration of colloidal particles, we can effectively and reversibly tune colloidal interactions to assume various steady-state configurations by changing the amplitude and frequency of the electric field.

Summary of the Most Important Results

II. Exploring colloidal configurations in the voltage-frequency phase space – transition from capacitive to resistive behavior

Metallic gold colloids were allowed to sediment onto the patterned electrode where they remain confined in a two-dimensional plane above the electrode surface due to gravity. The gold nanoparticles are electrostatically stabilized and do not aggregate in the dispersion or irreversibly attach to the underlying substrate during the experiment. In the absence of external electric fields, the gold colloids are Brownian and diffuse laterally over the electrode surface. The applied alternating current (AC) sinusoidal signal had frequencies in the range 10 Hz - 1 MHz and amplitudes in the range 0-5 V peak-peak. Three different electrode configurations were considered in this study, (i) interdigitating electrodes, (ii) interdigitating electrodes with conducting islands in-between, and (iii) a pointed electrode facing a flat electrode. The electrode configurations (ii) and (iii) were used to study the effect of non-uniform electric fields on colloidal transport and explore the possibility of engineering colloidal configurations with anisotropic electrical properties. The colloidal configurations were monitored using an optical microscope and charged coupled device (CCD) camera.

The equilibrium response of the colloidal system is determined by the interplay between gravity, Brownian motion and the driving forces induced by quasi-steady electrophoresis (EP), AC-electro-osmosis (ACEO), and dielectrophoresis (DEP) effects (explained in detail later in this report). Figure 2 shows the equilibrium response of 800-nm gold particles, suspended in 0.1-mM $NaHCO_3$ solution, to various electric field frequencies and amplitudes. We observe three distinct regions in the particle response. At forcing frequencies between 1~100 Hz, the particles go through quasi-steady electrophoresis EP), where they form a vertically spanning conducting wire oscillating between the two electrodes following the applied AC signal. Increasing the field amplitude increases the wire thickness, which in return reduces the effective gap between the two electrodes, and increases the circuit capacitance (compare Figs. 2i and 2a).

At moderate forcing frequencies (~ 1 kHz) we observe onset of AC electro-osmosis (ACEO), which forms an impinging flow at the center of the electrode gap that sweeps the particles towards the top of the electrodes. As explained by Morgan and Green, this motion is due to the fact that the fluid velocity is not

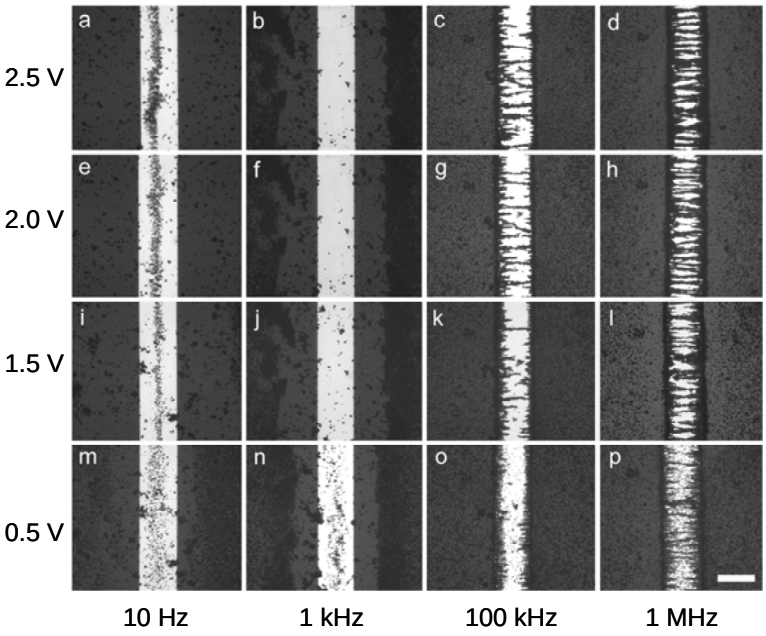

Figure 2. Equilibrium steady-state configurations of 800-nm gold colloidal particles at various electric field strengths and frequencies. At low forcing frequencies (1~100 Hz) quasi-steady electrophoretic response is observed, exhibiting increasing capacitance with increased field amplitude. At moderate forcing frequencies (~1 kHz) a 3-D flow is induced, which removes particles from the electrode gap. At higher frequencies, DEP overwhelms colloidal motion, and the colloidal circuit exhibits variable resistor behavior. Colloidal response time to reach the 2.5 V, 1-MHz equilibrium condition from a randomly distributed Brownian configuration was under 4 seconds. All equilibrium configurations were reversible and repeatable. The scale bar corresponds to 30 μm.

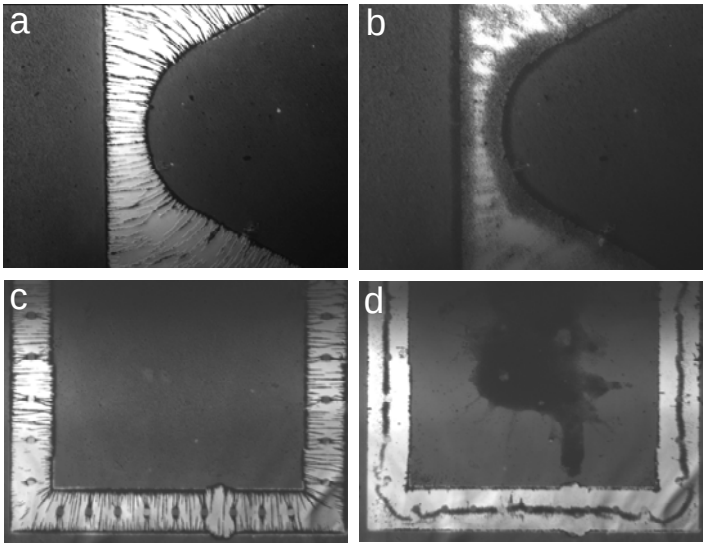

Figure 3. Reversible Au nanowire network formation with DEP in non-uniform electric fields (induced by a pointed electrode next to a planar conducting surface (a), and conducting islands between planar electrodes (c)) at 5 V peak-to-peak and 1 MHz . When the AC signal is changed to ω=100 Hz, the colloidal wires melt in (b), but shows an interesting response in (d) where a looping single wire connecting the intermediate gold bridges evolves from the configuration in (c).

constant across the electrode but is always a maximum at the edge where the field is highest. Therefore, ACEO can be used as an effective mechanism to remove particles from the electrode gap if necessary (see the 1 kHz column in Figure 2**)**. For ω>100 kHz, dielectrophoresis (DEP) becomes dominant, which enables formation of nanowires connecting the two electrodes. At 100 kHz, there are competing effects of DEP and AC-EO, which affects the number of nanowires in the microfluidic circuit (See the 100 kHz column in Figure 2). When the field amplitude was increased at this frequency, we observed a systematic increase in the number of nanowires. This can possibly be utilized to directly vary the circuit resistance. In contrast with the lower frequencies, we consistently observe larger number of nanowires at 1 MHz and the time taken to establish these conductive circuits is significantly reduced. Comparing the colloidal system responses at 1 MHz and at 1.5, 2 and 2.5 V, we observe more or less the same number of nanowires (see Figs. 2d, h and i). To give an idea about the system response times, it took under 4 seconds to reach the equilibrium configuration in Fig. 2d from a randomly distributed Brownian configuration. To put these results in perspective in terms of the system impedance, the microfluidic device can transition from a state where the impedance is purely reactive to a different state where the impedance is purely resistive within a few seconds, and all colloidal equilibrium configurations are completely *reversible* and *repeatable*.

Figure 3 shows reversible Au nanowire network formation with DEP in non-uniform electric fields at 5 V peak-to-peak and 1 MHz . The non-uniform electric fields were induced by a pointed electrode next to a flat conducting surface in Fig. 3a,b, and conducting islands between planar electrodes in Figs. 3b,d. When the AC signal was changed to ω=100 Hz, the colloidal wires melt in Fig. 3b, but shows an interesting response in Fig. 3d, where a looping single colloidal wire connecting the intermediate gold bridges evolves from the configuration in Fig. 3c in less than 30 seconds. This could potentially be useful in engineering colloidal configurations with anisotropic electrical properties. Further electrical property measurements are necessary to assess the utility of non-uniform electric fields in improving the electrical properties otherwise obtained with uniform electric fields.

III. Scaling analysis.

In the following, we present an analysis of colloidal particle dynamics and summarize the type of fluid flow observed in a simplified system consisting of two co-planar parallel gold electrode strips. The experimental results discussed in the previous section are put in perspective using a general understanding of scaling laws governing this simple system. Preliminary scaling arguments provided here are intended to provide some intuition and predictive capabilities for the frequency and amplitude dependent behavior of colloidal microstructures and their associated electromagnetic properties, and within limits, can be extended to more complicated microelectrode shapes. In addition, these scaling arguments suggest opportunities (and limits) for tuning device characteristics over a broad range based on available colloidal fluid characteristics (e.g. particle size, shape, dielectric properties; fluid viscosity, dielectric properties; other parameters - temperature, micro-channel dimensions, etc.).

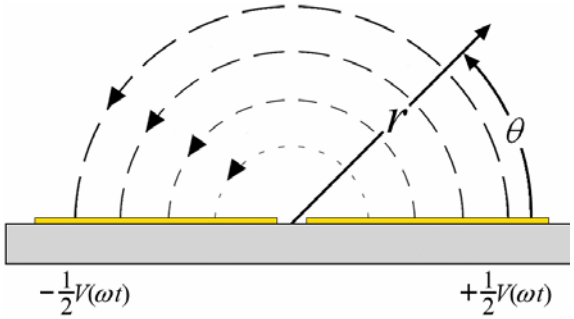

Figure 4. Schematic of a simplified co-planar gold electrode system showing the electric field lines. The electric field in this arrangement is a function of r and θ.

The gold colloids used in this work have a radius a=400 nm, and were suspended in an aqueous ionic solution with a conductivity, σ=9 μs/cm. Typical system lengths of the microelectrodes (inter-electrode gaps) used in this study varied between 35 and 50 μm. The AC signals applied to these electrode systems were up to 10 V peak-to-peak, giving rise to field strengths as high as 5 x 10^6 V/m. The

applied signals had frequencies in the range, ω=10 Hz – 1 MHz.

A schematic diagram of the microelectrode system used in this work with the electric field lines is shown in Fig. 4. As the spacing between the electrodes is small compared to the length and width of the electrodes, the system is essentially two-dimensional. This simplified set-up serves as an ideal test case to explore the relative magnitudes of different forces in play, and the validity of assumptions made in the scaling analysis. This systematic study is potentially important as we try to extend the results to experimentally more complex electrode arrangements.

It is important to distinguish the motion of particles caused by gravity, Brownian motion, electrophoresis (EP), and dielectrophoresis (DEP), from the liquid motion in the microelectrode structures due to mechanical, electrical (AC electroosmosis (AC-EO), etc.), and thermal (Joules heating, etc.) effects. The interplay of these forces and their relative contributions determine dominant forces for different conditions and the resulting behavior and properties of colloidal fluids. In this analysis, we particularly look at relative magnitudes of particle velocities due to different forces acting on the particle to identify the dominant transport mechanism. Direct expressions for the displacements of a single isolated particle in the microelectrode system due to the forces mentioned above are provided; the analysis does not take into account particle-particle interactions or multi-body hydrodynamic interactions.

Gravity is a conservative force that always acts on a colloidal particle suspended in a fluid. For a particle of density ρ_p suspended in a medium ρ_m, the displacement due to the gravitational field, Δx_g, can be obtained by equating the buoyant force and the Stokes drag, and is given by:

$$\Delta x_g = \frac{2}{9}\frac{a^2\left(\rho_p - \rho_m\right)g}{\eta}t, \tag{1}$$

where t is the time, g is the acceleration due to gravity and η is the fluid viscosity. The colloidal particle sediment on to the electrode surface due to gravity and assumes an equilibrium position that is dictated by a balance of the gravitational force and the electrostatic repulsion between the particle and the electrode. The gravitational settling time for 400 nm gold particles in water at 25 °C is around 2 minutes. In all experiments in this work, electric fields are applied only after the colloidal particles have sedimented onto a two-dimensional plane close to the electrode surface; as a result gravity has a minimal role on the lateral transport of colloidal particles in the two-dimensional plane.

Another force relevant to colloids is the random Brownian force, which is characterized by the thermal energy, kT, which depends only on the temperature (T). For example, colloidal diffusion is determined by the balance of Brownian and hydrodynamic drag forces as characterized by the Stokes-Einstein diffusion coefficient ($D=kT/6\pi\mu a$), and the Brownian displacement (in one dimension) is given by:

$$\Delta x_B = \sqrt{2Dt} = \sqrt{\frac{kT}{3\pi a\eta}t}. \tag{2}$$

However, when a colloidal particle is near a wall or surrounded by other particles, in a microfluidic channel for instance, the diffusion coefficient is proportional to a^{-2} due to hydrodynamic interactions between the two surfaces. To move a particle in a deterministic manner, a force greater than the random Brownian force is necessary.

Colloidal particles in an external AC electric field are subjected to electrophoretic and dielectrophoretic forces. For thin electric double layers, the electrophoretic mobility is given by the Smoluchowski equation, $u=\varepsilon\zeta E/\eta$, where ε and ζ are the electrical permittivity and the zeta potential of the particle. Integrating the Smoluchowski equation for a sinusoidal time-dependent bias, we can obtain the particle trajectory as a function of time due to quasi-steady electrophoresis:

$$\Delta x_{EP} = \frac{\varepsilon\varsigma}{\omega\eta}\frac{V}{r}\cos\left(\omega t\right), \tag{3}$$

where V is the peak-to-peak voltage and r is the spacing between the electrodes. In AC fields, the particle

displacements are oscillatory and follow the AC signal at low frequencies, and are negligible at higher frequencies.

Dielectrophoresis arises from the interaction of induced dipoles on polarizable colloidal particles with a spatially non-uniform electric field. In contrast to electrophoresis, dielectrophoretic force has a non-zero time average, and leads to a finite particle displacement even at high AC frequencies. The DEP induced displacement of a spherical particle can be given by:

$$\Delta x_{DEP} = \frac{a^2 \varepsilon}{6\eta} \mathrm{Re}\left[\frac{\tilde{\varepsilon}_p - \tilde{\varepsilon}}{\tilde{\varepsilon}_p + 2\tilde{\varepsilon}}\right] \nabla |E|^2 t, \qquad (4)$$

where $\tilde{\varepsilon}$ is the complex permittivity. The expression in brackets is the Claussius-Mossotti factor and takes a value between +1 and -1/2, depending on the direction of DEP; particle moves towards (positive DEP) or away from (negative DEP) the regions of high electric field strength, depending on the frequency. For the simplified electrode geometry considered in Fig. 4, the exact solution for the electric field when the electrodes are semi-infinite with an infinitely small gap can be used. Assuming a Claussius-Mossotti factor of 1, the displacement due to DEP reduces to:

$$\Delta x_{DEP} \approx 0.03 \frac{a^2 \varepsilon}{\eta} \frac{V^2}{r^3} t, \qquad (5)$$

where V is the amplitude of the applied voltage and r is the distance of the particle from the center of the gap. For anisotropic colloids having more than one length scale (e.g. major and minor axis of rod shaped particles), there will also be more than one distinct force and time scale associated with each relevant length scale.

Interactions of the tangential electric field with the induced charges on each electrode result in AC electroosmotic force and steady fluid flow (nonzero time averaged) with a velocity that depends on both the applied potential and frequency. As the tangential electric field is larger near the edges of the electrodes, the electroosmotic velocity is also large at these locations, and decays away from the electrode edges. Changing the electrode polarity does not change the direction of the AC electroosmotic force (flow is unidirectional). From the work of Green and co-workers, we can write the particle displacement due to AC-EO as:

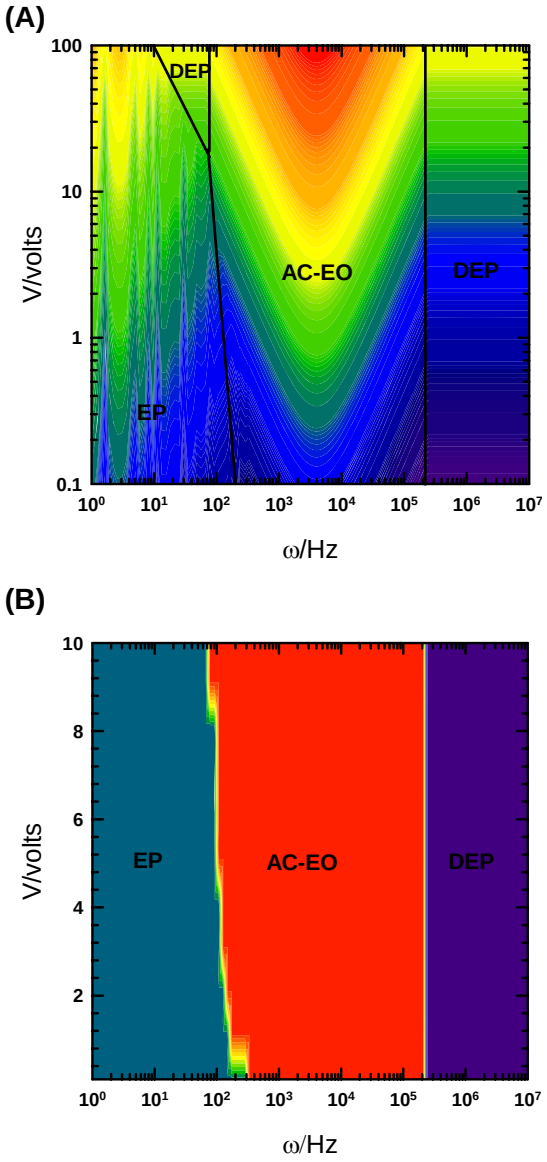

Figure 5. (A) A voltage-frequency phase diagram of particle velocity for a gold colloid with radius a = 400 nm in a medium with conductivity, σ=9 μS/cm. The velocity contours are in units of m/s, (B) A voltage-frequency phase-diagram similar to Fig. 5A, where the particle velocity contours are replaced by a color code to identify the dominant transport mechanism at a given voltage and frequency. Quasi-steady electrophoresis (EP) is the dominant transport mechanism at low frequencies (ω<100 Hz), while AC electroosmosis (AC-EO) is active at moderate frequencies (100 Hz<ω<100 kHz) and dielectrophoresis dominates at higher frequencies (ω>100 kHz).

$$\Delta x_{AC-EO} = \Lambda \frac{\varepsilon V^2}{8\eta r} \frac{\Omega^2}{\left(1+\Omega^2\right)^2} t$$
$$\Omega = \Lambda \frac{\omega \varepsilon \pi r}{2\sigma \kappa^{-1}};\ \Lambda = \frac{C_S}{\left(C_S + C_D\right)} \quad (6)$$

where κ^{-1} is the Debye length and is about 30 nm for all experiments in this study, C_S and C_D are the capacitance of the Stern layer and diffuse layer, and $\Lambda \approx 0.2$ for a gold electrode system.

Figure 5A shows the domains of influence of different electrokinetic forces (DEP, EP, AC-EO) acting on a 400 nm gold colloidal particle in a voltage-frequency phase diagram. The contours represent displacement per second due to the dominant transport mechanism and have units of m/s. In Fig. 5B, the particle velocity contours are replaced by a color code to identify the dominant transport mechanism at a given voltage and frequency. The range of voltage and frequencies considered in the scaling analysis are similar to the values used in the experiments to allow direct comparison. It can be seen from Fig. 5 that quasi-steady electrophoresis (EP) is the dominant transport mechanism at low frequencies (ω<100 Hz) for voltages less than 20 V, while AC electroosmosis (AC-EO) is active at moderate frequencies (100 Hz<ω<100 kHz) in the entire voltage range and dielectrophoresis dominates at higher frequencies (ω>100 kHz) for all voltages. It is also interesting to note the presence of a small DEP domain in the low-frequency phase space for voltages greater than 20 V in Fig. 5A. It is to be noted that frequency dependent electrothermal effects and Joules heating that become important at high voltages were not considered in this analysis, and the appearance of the small DEP zone at low frequencies could be a manifestation of this omission. The experimental results in Fig. 2 serve as a direct validation of the scaling analysis. The equilibrium colloidal configurations formed at different voltages and frequencies can be attributed to the dominant transport mechanism identified in Fig. 5. Quasi-steady EP was responsible for concentrating the particles in-between the electrodes at ω<100 Hz, and the magnitude of particle displacements due to EP increased as the voltage increased, resulting in a greater number density of colloidal particles in the region in-between the electrodes. At moderate frequencies, 100 Hz<ω<100 kHz, we observed a circular flow pattern centered around the edges of the electrodes set up due to AC-EO, that resulted in flushing out the gold colloids from the region in-between the electrodes onto the gold electrode surface. At higher frequencies (ω>100 kHz), the colloidal particles formed conducting chains that bridged the gap between the electrodes. The conducting wire networks formed faster when the voltage was increased due to an increase in the DEP force. It is encouraging that a simple scaling analysis that neglects many-body interactions can be used to consistently capture experimental observations of colloidal particle transport in simple microelectrode geometries. It would be interesting to test its validity in more complex electrode geometries.

IV. Electrical property measurements

In this section, we report the electrical property measurements of colloidal configurations assembled over a planar electrode system (Fig. 2), as a function of frequency. The two colloidal configurations of interest are 1) “resistive circuit” formed in Fig. 2d and, 2) “capacitive circuit” formed in Fig. 2a. In particular, we measure the impedance (Z) that represents the total opposition offered by a device or circuit to the flow of AC current at a given frequency. The capability to manifest significant changes in the impedance characteristics, by tuning colloidal configurations in a controllable fashion is a powerful tool that renders itself to many applications involving active nanostructures.

Impedance is a complex quantity that consists of a real part (resistance, R) and an imaginary part (reactance, X). In general, the impedance of a device or circuit is written as:

$$Z = R + jX \quad (7)$$

The reactance takes two forms – inductive (X_L) and capacitive (X_C). By definition, $X_L=\omega L$ and $X_C=1/\omega C$, where ω is the angular frequency of interest, L is the inductance and C is the capacitance.

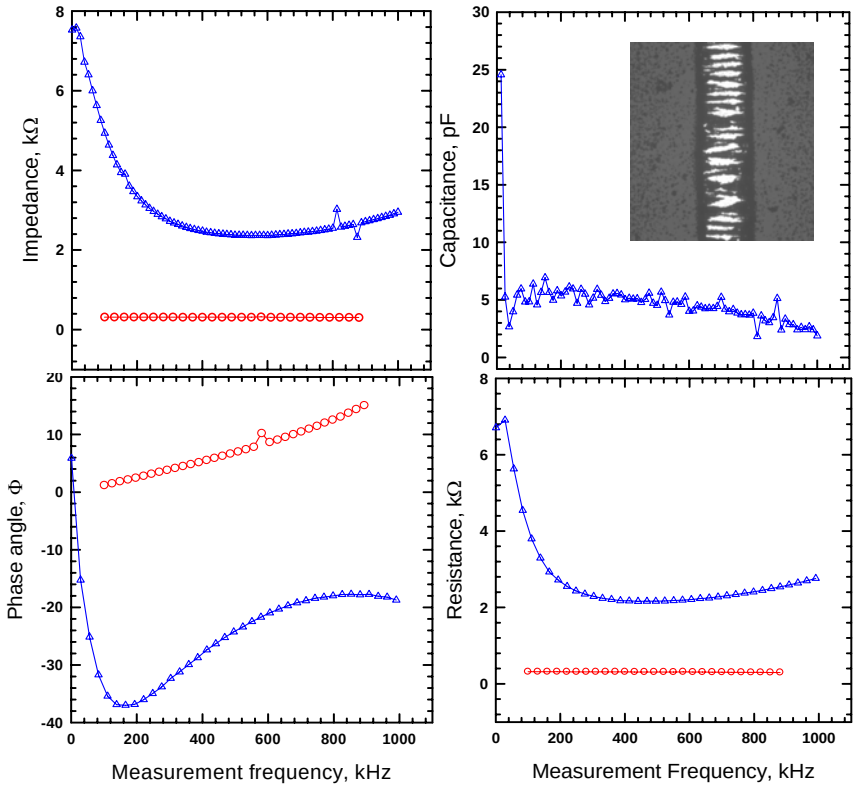

Figure 6. The impedance, phase angle, capacitance and resistance of the colloidal configuration corresponding to a "resistor" assembled in the planar gold electrode system at 2.5 V, 1 MHz (shown in inset) plotted as a function of frequency. The blue triangle correspond to measurements made when there is no external forcing, and the red circles correspond to frequency sweep measurements made when an external AC signal is applied to assemble the colloidal gold into nanowires.

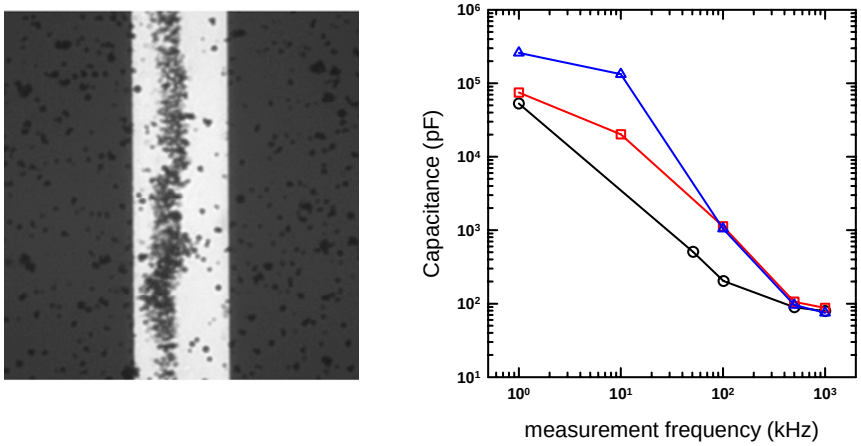

Figure 7. The capacitance of the colloidal configuration corresponding to a "capacitive" circuit assembled in the planar gold electrode system at 2.5 V, 10 Hz (shown in Fig. 7a) plotted as a function of frequency. The black circles correspond to the capacitance of 0.1 mM $NaHCO_3$ solution without gold nanoparticles, the red squares correspond to the capacitance 0.1 mM $NaHCO_3$ solution seeded with 800 nm gold particles when there is no external forcing, and the blue triangles correspond to frequency sweep measurements made when an external AC signal is applied to assemble the colloidal gold into vertically spanning nanowires inbetween the electrodes.

The impedance of the electrode/electrolyte/gold nanoparticle system was measured with an Agilent HP 4194A impedance analyzer. The analyzer was connected in series with the function generator used to actively assemble the gold nanoparticles. As the colloidal configurations formed are sensitive to the applied AC frequency, care was taken to make sure that the frequency sweep performed by the analyzer does not alter the assembled configurations. The voltage applied by the analyzer was 0.5 V. The frequency sweep to measure the electrical properties was initiated only after the assembly of the colloidal particles into the desired configuration was complete. A data acquisition system controlled by a LABVIEW program was used to record the electrical property measurements real-time. Multiple frequency sweeps were performed to check the reproducibility of the measurements.

Figure 6 shows a representative set of electrical property measurements obtained after a frequency sweep was performed with the impedance analyzer. The properties correspond to the colloidal configuration with gold nanowires shown as an inset in Fig. 6b, and are compared with the corresponding values for the electrolyte solution seeded with gold nanoparticles when there is no external forcing. The data shows that the impedance, phase angle, capacitance and resistance are functions of frequency. When there is no external forcing, the capacitance tends to a constant value at frequencies greater than 100 kHz, equivalent to that of a parallel plate capacitor with the permittivity of the bulk electrolyte containing a known volume fraction of gold nanoparticles (Fig. 6b). Similarly, the resistance can also be seen to be fairly constant at high frequencies, with a value that is inversely proportional to the conductivity of the solution seeded with nanoparticles (Fig, 6d). These limiting values correspond to the impedance of the bulk electrolyte with gold nanoparticles, since at high frequencies the electric double layer impedance is negligible. At low frequencies, the total measured resistance and capacitance includes the impedance of the double layer (Fig. 6b, d). The negative phase angle at all frequencies indicates that the circuit is predominantly capacitive in nature. However, when an external electric field that results in the formation of conductive gold nanowire bridges is applied, the device switches from a pure capacitive circuit to a resistive circuit. This can be seen from the constant resistance of R=300 Ω, recorded as a function of frequency in Fig. 6d. For a pure resistor, the resistance is independent of frequency and the phase angle is zero at all frequencies. However, in our experiments the phase angle measured was finite and positive and a function of frequency (Fig. 6c). This suggests the possibility of the device having a non-zero inductance, as inductors have a positive phase angle. It also has to be kept in mind that all circuit components are neither purely resistive nor purely reactive, and are a combination of these impedance elements. As a result all impedance measurements have parasitic contributions; for eg. unwanted inductances in resistors, unwanted resistance in capacitors, or unwanted capacitance in inductors, etc., which can also be seen in our experimental measurements. Negative values of capacitance were measured at all frequencies for this configuration and are therefore not plotted in Fig. 6b. A possible explanation for recording negative capacitance could be the following: All components have a self-resonant frequency due to the parasitics of the component. As the frequency is increased, a capacitor's impedance will change and will start to look like a series capacitor/inductor/resistor. At some point, the reactance due to the inductance exceeds the reactance due to the capacitance and the capacitor looks more like an inductor. This argument is in some sense validated by the positive phase angles recorded, indicating inductive behavior. Nevertheless, the plots in Fig. 6 show the ability to change the impedance characteristics of the system by facilitating a change in the colloidal configuration.

We also performed capacitance measurements in the circuit by forcing the microfluidic system at 10Hz and 2.5 V, and measuring the system impedance in series to the actuation signal, at frequencies spanning from 1 kHz to 1 MHz. Figure 7b plots the capacitance in pF as a function of frequency for 1) 0.1 mM NaHCO3 solution without gold nanoparticles, 2) 0.1 mM $NaHCO_3$ solution seeded with 800 nm gold particles when there is no external forcing, and 3) 0.1 mM $NaHCO_3$ solution seeded with 800 nm gold particles with external forcing resulting in the colloidal configuration shown in Fig. 7a. It can be seen that all three capacitance curves tend to the same constant value at high frequencies, equivalent to that of a parallel plate capacitor with the permittivity of the bulk electrolyte. Addition of gold nanoparticles to the sodium bicarbonate solution increased the capacitance at low frequencies, while having negligible effect at high frequencies. The results also show a four fold increase in capacitance from its base-line value

obtained under zero forcing, when a vertically spanning colloidal wire assembles in the center of the gap between the electrodes (Fig. 7a).

Listing of all Publications:

Beskok A., Bevan, M.A., Lagoudas, D., Ounaies, Z., "Reversible Control of Anisotropic Electrical Conductivity using Colloidal Microfluidic Networks," Interim Progress Report, Submitted to the ARO

List of all participating scientific personnel

Ali Beskok,
Michael Bevan,
Dimitris Lagoudas
Zoubeida Ounaies
Pradipkumar Bahukudumbi
William Everett